Using remote sensing to assess the effect of trees on millet yield in complex parklands of Central Senegal

L. Leroux, G.N. Falconnier, A.A. Diouf, B. Ndao, J.E. Gbodjo, L. Tall, A.A. Balde, C. Clermont-Dauphin, A. Bégué, F. Affholder, et al.

Using remote sensing to assess the effect of trees on millet yield in complex parklands of Central Senegal

Leroux L[1,2,±]., Falconnier G.N[2,3]., Diouf A.A[4]., Ndao B[4]., Gbodjo J.E[5]., Tall L[6]., Balde A.A[7]., Clermont-Dauphin C[8,9]., Bégué A[10,11]., Affholder F[2,3]., Roupsard O[8,9,12].

1. CIRAD, UPR AIDA, Dakar, Senegal
2. AIDA, Univ Montpellier, CIRAD, Montpellier, France
3. CIRAD, UPR AIDA, Montpellier, France
4. Centre de Suivi Ecologique, Dakar, Senegal
5. INRAE, UMR TETIS, Univ Montpellier, Montpellier, France
6. Laboratoire National de Recherches sur les Productions Végétales, ISRA, Dakar, Senegal
7. SODAGRI, Dakar, Senegal
8. Eco&Sols, Univ Montpellier, CIRAD, INRAE, IRD, Montpellier SupAgro, Montpellier, France
9. LMI IESOL, Centre IRD-ISRA de Bel Air, BP1386, CP18524 Dakar, Senegal
10. CIRAD, UMR TETIS, F-34398, Montpellier, France
11. TETIS, Univ Montpellier, AgroParisTech, CIRAD,CNRS, INRAE, Montpellier, France
12. CIRAD, UMR Eco&Sols, BP1386, CP18524, Dakar, Sénégal

± Corresponding author : louise.leroux@cirad.fr

Abstract:

Agroforestry is pointed out by the Intergovernmental Panel on Climate Change report as a key option to respond to climate change and land degradation while simultaneously improving global food security (IPCC, 2019). *Faidherbia albida* parklands are widespread in Sub-Saharan Africa and provide several ecosystem services to populations, notably an increase in crop productivity. While remote sensing has been proven useful for crop yield assessment in smallholder farming system, it has so far ignored the woody component. We propose an original approach combining remote sensing, landscape ecology and statistical modelling to i) improve the accuracy of millet yield prediction in parklands and ii) identify the main drivers of millet yield spatial variation. The parkland of Central Senegal was chosen as a case study. Firstly, we calibrated a remote sensing-based linear model that accounted for vegetation productivity and tree density to predict millet yield. Integrating parkland structure improved the accuracy of yield estimation. The best model based on a combination of Green Difference Vegetation Index and number of trees in the field explained 70% of observed yield variability (relative Root Mean Squared Error (RRMSE) of 28%). The best model based solely on vegetation productivity (no information on parkland structure) explained only 46% of the observed variability (RRMSE=34%). Secondly we investigated the drivers of the spatial variability in estimated yield using Gradient Boosting Machine algorithm (GBM) and biophysical and

management factors derived from geospatial data. The GBM model explained 81% of yield spatial variability. Predominant drivers were soil nutrient availability (*i.e.* soil organic nitrogen and total phosphorous) and woody cover in the surrounding landscape of fields. Our results show that millet yield increases with woody cover in the surrounding landscape of fields up to a woody cover of 35%. These findings have to be strengthened by testing the approach in more diversified and/or denser parklands . Our study illustrates that recent advances in earth observations open up new avenues to improve the monitoring of parkland systems in smallholder context.

Keywords: Agroforestry; landscape; crop yield; smallholder agriculture; remote sensing; Faidherbia albida; Africa

1 Introduction

Scientific and political spheres agree on the need to foster the inclusion or upholding of trees in agricultural systems, in order to tackle the social and environmental dimensions of the sustainable development goals (SDGs, United Nations, 2016). Agroforestry, *i.e.* the combination of trees and crops or pastures on the same piece of land (Nair, 1993) has been acknowledged as an option to respond to climate change and land degradation (IPCC, 2019).

In sub-saharan Africa, around 40% of people in rural areas live in landscapes with more than 10% tree cover, often agroforestry systems (Zomer et al., 2014). In semi-arid West Africa, traditional parklands are characterized by the deliberated retention of trees on agricultural land (Boffa, 1999) due to the socio-ecosystem services they provide (Sinare and Gordon, 2015). Parklands contribute to the conservation of natural resources and biodiversity, and improve soil fertility and agricultural productivity (Baudron et al., 2019; Bayala et al., 2014; Duriaux Chavarría et al., 2018; Peltier, 1996). Trees compete with crops for resources but they can improve nutrient cycling, soil moisture retention and microclimate (*e.g.* Kho et al., 2001; Sida et al., 2018).

Studies on the impact of tree on crop productivity were generally conducted at tree-scale where crop performance under tree crown was compared with crop performance in a control area without tree influence (Bayala et al., 2015). Tree density in West African parklands is often very high and some tree

species can influence crops beyond their crown (sometimes more than 100 m²/tree, Sileshi, 2016). Finding a control area without tree influence can thus be challenging, which can bias the quantification of trees influence on crops. In addition, parklands are composed of combinations of tree species with different densities and spatial arrangement. Synergies or antagonisms occur between trees and trees effect on crop performance is not likely to be additive. The direction and magnitude of the impact of trees on crop productivity depends on the dominant tree and crop species, and management practices. For instance, nitrogen-fixing *Faidherbia albida,* was found to improve millet and wheat yield (Bayala et al., 2012; Kho et al., 2001; Louppe et al., 1996; Sida et al., 2018) but not groundnut yield (Louppe et al., 1996). In Burkina-Faso, millet performed better under *Adansonia digitata* than *Parkia biglobosa*, the latter being a shading-tree (Sanou et al., 2012). The presence of *Grevillea robusta* in maize and wheat fields decreased fertilizer use efficiency while the presence of *F.albida* improved it (Sida et al., 2019).

Though parklands have been the focus of researches for several decades, few studies have tackled the question of the landscape-scale effect of parklands on crop productivity. Research in Ethiopia on the effects of *F.albida* on barley yields according to different land use systems (Hadgu et al., 2009), and agricultural productivity along a forest-agriculture gradient (Baudron et al., 2019; Duriaux Chavarría et al., 2018) are rare example.

The inter-connection of social, environmental and economic challenges as committed by the SDG calls for systemic and integrated approaches in which landscape scale is particularly appropriate to inform decision making (Reed et al., 2016). Remote sensing provides physical measurements of temporal and spatial development of agroforestry systems (*e.g.* structure, biomass). It could help account for tree-crop interactions and the resulting impacts on crop productivity. Current statistical models establish relationships between remote sensing vegetation productivity indices and *in-situ* yields measurements or national agricultural statistics. Until recently, crop growth monitoring and crop yield mapping in smallholder agriculture have relied mainly on low spatial resolution images covering large areas (Leroux et al., 2019, 2016; Maselli et al., 2000; Mkhabela et al., 2005; Rasmussen, 1992). However, in agroforestry parklands across sub-Saharan Africa, accurate estimates of crop yields are hampered by landscape fragmentation, fields being often smaller than one hectare (Fritz et al., 2015). Diversity in soil conditions,

crop management and tree conservation practices further amplifies inter and intra-field yield variability. New satellite or low-cost nanosatellite sensors with high spatial resolution (≤ 10 m) and high revisit frequency (< 2 weeks) are more suited to these complex and spatially variable agricultural systems. These new sensors open unprecedented opportunities to predict and map crop yield in smallholder context. A promising crop yield mapping at field level have been obtained for East and West African farming systems using Sentinel-2, Sentinel-1 and PlanetScope data (Burke and Lobell, 2017; Jin et al., 2019, 2017; Lambert et al., 2018). However these studies masked out trees to capture 'pure cropped pixels' (Lambert et al., 2018) and thus masked-out the crop below tree crown and neglected the influence of the tree on crops beyond its crown projection. Though promising, these approaches have usually failed to fully reproduce the wide variability in observed crop yield in farmer fields in sub-Saharan Africa (*e.g.* Jin et al., 2019; Lobell et al., 2019).

Combining information on vegetation productivity and parkland structure derived from high spatial resolution, satellite images offers the opportunity to capture the variability in crop yield in parkland systems and to identify where and how crop productivity could be improved. Remote sensing have been extensively used to identify and analyzed yield gap (*i.e.* the difference between observed actual yields and water-limited yields) (*e.g.* Jain et al., 2017; Jin et al., 2019; Löw et al., 2017; Zhao et al., 2015). In Kenya, Jin et al. (2019) explained more than 70% of maize yield variability by edaphic drivers using remote sensing, crop process-based modelling and machine learning. In parkland systems, analyzing drivers of yield spatial variability could help assess relevant opportunities to optimize parkland management.

The main aim of this study was to assess the role of trees in explaining spatial variations in millet yield in a case-study agroforestry parkland dominated by *Faidherbia albida*, in the Groundnut Basin of Senegal. To do so, we used high spatio-temporal resolution images (Sentinel-2, PlanetScope and RapidEye) and ground-observations. More specifically, we addressed three questions: (i) Does information on parkland structure (i.e. number of trees per field, tree density, and percentage of tree cover) help improve the accuracy of millet yield prediction in parklands of central Senegal? (ii) What are the main drivers of the predicted spatial variability in millet yield?, and (iii) What is the relative influence of trees compared with the other identified drivers?

We thus propose an original approach combining remote sensing, field data and statistical modeling. This approach was tested for an agroforestry parkland dominated by *Faidherbia albida*, in the Groundnut Basin of Senegal.

2 Materials and Methods

2.1 Study area

The study was conducted in 2017 and 2018 in Senegal. The study area (~17 km²) is located in a village named Diohine. The village is at the centre of the main rainfed agriculture area of Senegal (Fig 1a), the "Old Groundnut Basin". This name refers to the economic importance of groundnut in the region, since colonial times.

The climate is sudano-sahelian, with annual rainfall ranging from 400 mm to 650 mm. An increasing trend in annual rainfall has been observed since the 1990's (Lalou et al., 2019), after a long period of low annual rainfall. The rainy season lasts from July to October, August and September being the wettest months. Annual rainfall was 490 mm and 447 mm in 2017 and 2018 respectively (see supplementary material S1 for in-season distribution). Soils are sandy, developed on quaternary wind sediments. Dominating sandy 'dior' soils are spread over flat and dune areas, while slightly more clayish 'dek' soils are located in inter-dunes and lowland areas (Lericollais, 1999).

Livelihoods of rural populations are centered on small-scale rainfed agriculture with low external input use. The study area is characterized by tree-based cropping systems, hereafter referred as parklands. *Faidherbia albida* (also called 'Kadd' in Wolof or 'Sas' in Serer) cohabitates with crops. *F.albida* is a leguminous nitrogen-fixing species that relies on deep groundwater. Its vegetation period spreads over the dry season whereas most other local plant species grow during the rainy season. *F. albida* sheds leaves at the end of the dry season which (i) reduces direct competition for light with crops compared with other tree species, and (ii) provides green manure that contributes to increase soil fertility and crop yield under tree crown. This 'fertility hotspot' is also termed the 'albida effect' (see the review of Sileshi, 2016). However, *F.albida only* represents 34% of trees in the region. The parkland is diversified with 24 species in total. *Adansonia digitata* and *Ziziphus mauritania* account for 16% and 10% of species respectively. The main crops are pearl millet (*Pennisetum glaucum* (L.) R. Br.) (37% of study area) and groundnut (*Arachis hypogaea* L.) (22% of study area) (Fig 1b). Millet is grown for on-farm consumption while groundnut is a cash-crop. 'Home fields', close to homesteads, are mainly cultivated with

147 continuous pearl millet while remote 'bush fields' are cultivated with pearl millet and groundnut in biennial
148 rotation. In Diohine, unlike in most of the other villages in the region, 'bush fields' are still fallowed as part of a
149 triennial rotation with pearl millet and groundnut. Other crops are sorghum (*Sorghum bicolor* (L.) Moench),
150 cowpea (*Vigna unguiculata* L.) and bissap (*Hibiscus sabdariffa*), that can be cultivated as sole crop or
151 intercropped with pearl millet. Pearl millet is mostly cultivated on 'dek' soils and generally sown in June, before
152 the first rain and harvested from October to November depending on the cultivar (Fig 2). Crop management is
153 performed with animal draught power except for less-endowed farmers who lack equipment. Mineral fertilizer
154 use is low.

155 ## 2.2 Field data

156 50 farmers' fields (35 in 2017 and 15 in 2018) were monitored along a landscape gradient constituted of four
157 landscape classes. The landscape classes were defined based on remote sensing and a set of biophysical
158 variables (vegetation average productivity and inter-annual variability, evapo-transpiration, woody density
159 and soil texture (Ndao et al., 2019, 2018))(Fig 1c). Class 1 corresponds to less productive areas
160 characterized by saline soils. Class 2 is characterized by moderate vegetation productivity and low spatial
161 heterogeneity in vegetation productivity while class 3 has a greater spatial heterogeneity in vegetation
162 productivity indicating a more diversified landscape. Class 4 have a high woody cover and is dominated by
163 hydromorphic soils. Fields monitored in 2017 were mainly in landscape class 3. The landscape classes were
164 defined after the 2017 cropping season. In 2018, fields were selected randomly with a number of fields per
165 landscape class weighted by the share of the area of each class in the whole study area. Field boundaries
166 and individual tree location and species were recorded with a Garmin GSMAP 64 GPS device. Due to a
167 GPS-reported accuracy of 3-m, the location of each individual tree was adjusted by photo-interpretation of
168 Google Earth images (c). Within each field, three quadrats of 6-m² were selected, avoiding field
169 boundaries (> 3-m from the boundaries) and considering a contrasting range of distances to trees to cover
170 the intra-field yield heterogeneity induced by trees. Aboveground millet biomass was harvested within
171 each quadrat at crop maturity. Grain yield (dry matter) was measured after drying.

Fig 1

2.3 Satellite data preprocessing

Pearl millet cultivation occurs in the rainy season from May to October. High temporal resolution data are required to capture crucial changes in crop biomass on short time steps. We used optical images with high temporal resolution including Sentinel-2, PlanetScope and RapidEye data over 2017 and 2018 growing seasons to benefit from the high revisit capacity of each satellite and increase the probability of having cloud-free images over each growing season (Fig 2).

Sentinel-2A and 2B time series for the two growing season (temporal resolution of 5-days) were obtained from the Theia processing center at CNES (https://theia.cnes.fr/atdistrib/rocket). Sentinel-2 data were processed to level L2A using the MAJA processor providing ortho-rectified images, corrected from atmospheric disturbances and a cloud and cloud shadow mask (Hagolle et al., 2010). Among the 12 spectral bands provided by Sentinel-2, visible (blue, green, red), near infrared (NIR) and shortwave infrared (SWIR-2) bands, with a pixel size of respectively 10-m, 10-m and 20-m, were used. SWIR-2 band was resampled to 10-m spatial resolution using the nearest neighbor method.

Fig 2

Planet images were freely obtained from the PlanetScope constellation of nanosatellites operated by the Planet company (Planet-Team, 2018) as part of the Planet's Education and Research program. The PlanetScope constellation is currently composed of approximately 130 satellites and captures daily visible (blue, green, red) and NIR images (Planet-Team, 2018). We used the Level 3B PlanetScope Analytic Ortho Scene products, provided orthorectified with an approximately 3-m pixel size and a positional accuracy below 10-m Root-Mean-Square-Error (RMSE). The Planet data was converted to Top Of Atmosphere (TOA) reflectance using at-sensor radiance and supplied coefficients with each scene.

As for Planet images, RapidEye images were acquired through the Planet's Education and Research program. The RapidEye system is a constellation of five satellites with identical sensors and providing five-band multispectral images (blue, green, red, red-edge and NIR). We used the Level 3A RapidEye Analytic Ortho Tile Product with an ortorectified pixel-size of 5-m. The RapidEye data were converted to TOA reflectance using at-sensor radiance and supplied coefficient with each scene (Planet-Team, 2018).

From the initial set of images acquired during 2017 and 2018 growing seasons, only cloud-free images covering the sampled fields were used for millet yield estimation. We used a total of 25 images in 2017 and 31 images in 2018. Overall 2018 growing season was fully covered (Fig 2), with at least one cloud-free acquisition each month, while in 2017 no cloud-free images were available in September during millet grain filling.

2.4 Processing of multisources satellite time series

Six proxies of vegetation productivity were derived from the time series of multisource high spatial resolution optical images and three remote-sensing based proxies of parkland structure were derived from PlanetScope images at the beginning of the cropping season.

2.4.1 Proxies of vegetation productivity

Six vegetation indices (VI) were tested as proxies of vegetation productivity (Table 1). Excepted for the Normalized Difference Water Index that relies on Short Wavenlength Infra-Red (SWIR) only available for Sentinel-2, all VI were computed for each image of the multisource time series (Sentinel-2, RapidEye, PlanetScope). Mean VI values were computed for each of the monitored fields.

Table 1

To eliminate residual radiometric noise in VI time series due to poor atmospheric conditions, cloudiness masks and cross-sensors inconsistencies, field-scale VI time series were interpolated on a daily basis with a Whittaker smoother (Eilers, 2003). This usually results in a better match of the VI time series with crop growth (Duncan et al., 2015). VI cumulated over different periods in the growing season help account for asynchronic crop growth between fields due to space and time variability in environmental characteristics and management strategies (*e.g.* Leroux et al., 2019; Mkhabela et al., 2005; Rasmussen, 1992). Such

accumulations help remove signal short-term variations and improve estimates robustness. Two phenological parameters reflecting changes in plant growth were derived from smoothed daily profile of NDVI for each field based on a relative threshold method: (i) the onset of the greenness (SOS) and (ii) the end of the senescence (EOS). We used a modified version of the R software "greenbrown" package (Forkel et al., 2013) that allows to account for asymmetrical threshold between SOS and EOS. The two thresholds were tuned for each cropping season by comparing estimated SOS and EOS with the observed dates of emergence and senescence in the 50 surveyed fields. Overall, SOS and EOS were estimated with a mean absolute error below 10-days, except for EOS in 2017 (12-days; supplementary material S2). Overall accuracy of SOS and EOS estimates was greater for 2018 for which a more dense time series was available particularly around emergence in July (Fig 2). Errors were within the range of the satellite temporal acquisition and we assumed that the estimated phenological parameters were relevant to assess crop development variations in the study area. To identify the period that maximizes accuracy of yield estimates, the six smoothed vegetation productivity proxies were cumulated over different periods from SOS to EOS, with a 5-days time step and 5-days time shift.

2.4.2 Proxies of parkland structure

Three variables were tested as proxies of parkland structure: number of trees per field, tree density, and percentage of tree cover (hereafter refereed as woody cover). PlanetScope images with a resolution of 3-m were adapted to detect individual trees or cluster of trees. Number of trees per field, tree density per ha and woody cover were derived from PlanetScope image on 18 June 2017, *i.e.* at the beginning of the rainy season, when most tree species have their leaves and crops have not started growing. NDVI (see Section 2.4.1), indicator of green vegetation, was used to get a binary classification, i.e. "tree" (NDVI >0.16) or "no tree" (NDVI<0.16) at pixel level. This threshold value was obtained by visual screening. For each field, the number of trees was computed by detecting the number of patches of connected pixels based on the Queen's case contiguity measure. The estimated number of trees was in line with the observed number of trees in farmers' fields (R^2=0.78, P<0.001 with mean absolute error of 2.09). Tree density per ha was obtained by dividing the number of trees by field area. Woody cover was computed as the ratio of the number of tree pixels to the total number of pixels in the field. Due to the limited spectral resolution of

PlanetScope images, the identification of tree species was not feasible and therefore information related to parkland tree species composition was not included in the analysis.

2.5 Statistical analysis

2.5.1 Remote-sensing based models to estimate millet yield

Remote-sensing based regression models were calibrated with and without proxies of parklands structure (see 2.4.2) as input variables in addition to proxies of vegetation productivity proxies (see 2.4.1). For each vegetation productivity proxy (*i.e.* each six VI integrated over different periods), four linear regression models were calibrated: one model with vegetation productivity proxy alone and three models using an interaction term between vegetation productivity proxy and each of the three parkland structure proxies independently (*i.e.* woody cover, number of trees and tree density). More than 680 models were thus tested.

The models were calibrated using a 5-fold cross validation approach. Coefficient of determination (cv-R^2) and relative root mean square error (cv-RRMSE) were computed for each linear regression. To account for uncertainties in the dataset (*i.e.* measurement errors and residual noises in remote sensing observations), model parameters were optimized using the random sample consensus (RANSAC) algorithm. RANSAC allows to estimate iteratively model parameters from dataset that contains outliers (Fischler and Bolles, 1981). The minimum number of observations required to fit the models were set to 80% corresponding to 40 farmer fields.

2.5.2 Millet yield map and yield spatial variability analysis

A land use and land cover (LULC, Fig 1b) map of the study area was used to locate millet fields in 2018. The LULC map was derived from ground surveys and Sentinel-2 and PlanetScope images. The classification was achieved using a Random Forest algorithm (Breiman, 2001) implemented within the Moringa processing chain developed in the framework of the Theia Scientific Expertise Centre for land cover (https://www.theia-land.fr/en/ceslist/land-cover-sec/). The classification produced a LULC map with 85 % overall accuracy and with 77 % F-Score for millet (Ndao et al., 2019). Millet patch, defined as contiguous individual fields with similar biophysical and management characteristics, were obtained from an intersection of (1) object-based

segmentation of the study area into homogeneous patches using the multi-temporal PlanetScope NDVI data and (2) 2018 land cover and land use map. A majority voting was applied to extract the main LULC class in each patch. Millet yields were estimated for the entire study area in 2018 with the final best remote-sensing based model (see previous subsection). Proxies of vegetation productivity and parkland structure were computed for each millet patch.

Yield spatial variability (YH) was calculated by adapting equations proposed in Lobell and Azzari (2017) and Jin et al. (2019):

$$YH = (Y95 - Yest)/Y\,95 \quad \text{(Eq.2)}$$

where $Y95$ is the 95th percentile of estimated yields across millet patches over the study area and $Yest$ is the estimated yield of each millet patch. The 95th percentile of estimated yield was considered as the greatest attainable yield over the study area with current conditions.

A gradient boosting machine (GBM) algorithm (Friedman, 2001) was used to disentangle the contribution of biophysical and management factors in explaining crop yield variability. GBM is an ensemble learning technique that combine a large numbers of simple trees to optimize predictive performance and minimize overfitting risks (Friedman, 2001). GBM is a non-parametric approach that handles qualitative and quantitative variables. It is relatively insensitive to outliers and able to account for non-linear interactions between dependent and independent variables or between independent variables. Variables that contribute most to prediction accuracy can be identified with a relative influence measure. Functional relationships between predicted variables (yield variability in this study) and the independent variables can be obtained by visualizing the partial contribution of each independent variables, accounting for the average effect of the other variables (Friedman and Meulman, 2003). The R software and the "gbm" package (Greenwell et al., 2019) were used. The main parameters of the GBM model were set based on a grid search iterating over all possible combinations of parameters and assessing the top-performing combination (See supplementary material S3).

297 The driving factors used as independent variables in the GBM model to explain the estimated yield spatial
298 variability were (1) parkland structure within the millet patches and in their surrounding areas, (2) crop
299 water and nutrient stress and (3) soil characteristics (Table 2). Parkland structure in field surrounding
300 landscape can influence for instance pest regulation by natural enemies (Soti et al., 2019). To account for
301 this effect, mean woody cover and tree density (with no tree species distinction) in a buffer zone of 500-m
302 around each patch were calculated. Overall water stress over the growing season was derived from S2-
303 NDWI, overall nutrient stress over the growing season was derived from CIGreen and cover heterogeneity
304 over the growing season was derived from the mean variance Haralick feature (Haralick and Shanmugan,
305 1973). To investigate the effects of soil characteristics on the estimated yield spatial variability, the recently
306 released AfSoilGrids database (Hengl et al., 2017, 2015) was used. AfSoilGrids product are generated using
307 machine learning algorithms with soil samples from more than 50 0000 sites and a set of soil covariables used as
308 proxies for soil forming processes (landform, vegetation, lithology and climate). The accuracy of the prediction
309 was assessed using a 5-fold cross validation. Most of nutrients content are predicted with a coefficient of
310 determination greater than 0.5 (*e.g.* 0.61 for soil organic carbon, 0.66 for organic nitrogen and 0.85 for total
311 phosphorus).Soil texture, soil organic carbon content, organic nitrogen and total phosphorus in the topsoil
312 (0-30 cm) were extracted for each millet patch. All independent variables were aggregated at millet patch
313 scale using median value.

Table 2

314 3 Results

315 3.1 Millet yield estimation with remote sensing

316 3.1.1 Effects of parkland structure and vegetation productivity proxies, and integration
317 period on millet yield

318 Proxies of Vegetation productivity explained at least 50% (*i.e.* R^2>0.50) of millet yield variability (except
319 NDWI) (Fig 3a). NDVI and GDVI were the VI with the highest explanatory power corresponding respectively
320 to 32% and 27% of models with R^2>0.50. Greater accuracy was achieved when proxies for parklands
321 structure (*i.e.* number of trees, tree density and woody cover) were combined as explanatory variables in
322 the linear regression models (excepted for GDVI where some models based only on vegetation

productivity proxies exhibited R^2 above 0.50). Number of trees within fields was the prominent parkland structure variable (46% of models with R^2>0.50). The VI integration periods that maximized yield estimates accuracy were 5 to 15 days periods starting ~45 days after emergence and ending ~80 days after emergence (Fig 3b).

Fig 3.

3.1.2 Remote sensing-based model to estimate millet yield

Observed yields ranged from 351 kg/ha to 3278 kg/ha with standard deviation of 675 kg/ha. Depending on the vegetation productivity proxy, best models explained between 48 % and 70 % of millet yield variability. RRMSE varied from 36 % (RMSE=446 kg/ha) to 28 % (RMSE=348 kg/ha) (Fig 4a) and was substantially improved when proxies of parkland structure were included. The best improvement was observed for PSRINIR with a 10% decrease in RRMSE when considering parkland structure (Fig 4a and Fig 4b).

Fig 4.

The greatest R^2 was reached when GDVI was integrated over the 15 days between 50 and 65 days after emergence and combined with the number of trees within fields (Fig 4a and Fig 4c). For this latter, yields estimated with that best model agreed fairly well with field data (slope = 69, offset = 0.94). Marginal boxplots (Fig 4c) showed that observed and simulated yield had similar distribution. By comparison, the corresponding model without parkland structure information failed to reproduce the greatest yields (Fig 4d).

Fig 5

3.2 Drivers of yield spatial variability in parkland

Fig 5 shows the spatial patterns in estimated millet yields. Estimated yields at patch level over the study area for 2018 were small: median estimated yield was 720 kg/ha and 75% of the patches had a yield below 980 kg/ha (Fig 5a). Three spatial patterns were evidenced by Fig 5. Firstly, crop yield variation was high even between adjacent patches (Fig 5a). Yield ranged from less than 10 kg/ha to 2750 kg/ha (coefficient of variation = 61%). When effects of trees were not included, spatial variability was smaller (coefficient of variation = 36%), estimated yields ranging from 45 kg/ha to 2040 kg/ha with a median yields of 842 kg/ha

(Fig 5c). With this model, yield estimates in patches with high tree density and low tree density (see tree class on Fig 1b) were respectively smaller and greater than yield estimates with the model accounting for tree effect. Secondly, best yields were achieved close to the houses of Diohine and Kotiokh, at the extreme south-west of our study area, corresponding to what it is commonly called 'the fertility ring'. Patches at the south-east of Diohine on predominantly salines soils had low yields (Fig 5a). Thirdly, the size of the yield gap (*i.e.* the deviation from the 95th percentile) was substantial. The greatest estimated yields (95th percentile) in 2018 was 1912 kg/ha (Fig 5b). The majority of patches had yield between 53 % and 73 % of this best estimated yield (median value of 63 %).

GBM predictions of millet yield spatial variability were fairly accurate (R^2=0.81) (Fig 6a). A substantial proportion of the explained variance was due to three factors (with relative influence>15%) including soil characteristics (soil organic nitrogen and total phosphorus) and woody cover in the surrounding landscape of patches (Fig 6b). Yields in millet patches with soil organic nitrogen below 900 ppm tended to be lower than the highest estimated yields in the 2018 conditions and the probability to reach the highest yields increased with the soil organic nitrogen content (Fig 6c). A woody cover of ~30 - 40% in the surrounding landscape of patches maximized the positive impact of trees on crops. The probability of high deviation from the 95th percentile decreased with increase in woody cover until 30-40% woody cover and then increased for woody cover higher than 40% (Fig 6d).

Fig 6

4 Discussion

4.1 Integrating information on parkland structure improves yield prediction

Our study combined for the first time parkland structure variables with vegetation productivity proxies. We found that a model combining GDVI index integrated over 50-65 days after emergence and within-field number of trees explained 70% of millet yield variability (RMSE=348 kg/ha). Regardless of the vegetation productivity proxies considered, including proxies of parkland structure improved the accuracy of remote sensing based models (Fig 3a and Fig 4c). A major challenge in agroforestry parkland modelling is to account for the interaction between trees spatial arrangement and crops. Thus, trees and crops spatial

371 arrangement at plot or landscape scale, and their management (*e.g.* pruning) influences competition for
372 resources (Luedeling et al., 2016) and hence field-scale crop productivity. For instance, fruit trees such as
373 *Adansonia digitata* are mainly found closed to homesteads due to their crucial role for food security. In
374 addition, the influence of certain species such as *F.albida* extends beyond the canopy projection area due
375 to large lateral root system (Sileshi, 2016). This creates spatial variability in the availability of water and
376 nutrient for crops and consequently intra-field yield variability. The remote-sensing based model proposed
377 in this study accounted for this variability and fully captured the wide range of observed millet yields in the
378 study area. This is a strong improvement compared with previous studies conducted in similar landscape
379 that overlooked parkland structure information (*e.g.* Burke and Lobell, 2017; Jin et al., 2019; Lobell et al.,
380 2019).

381 Green Difference Vegetation Index (GDVI) outperformed the well-known Normalized Difference
382 Vegetation Index (NDVI; Fig 4a). Contrary to NDVI, GDVI is based on the green wavelength that is more
383 sensitive to variations in leaf chlorophyll concentration than the red wavelength (Daughtry et al., 2000;
384 Gitelson et al., 2005). Leaf chlorophyll concentration is a proxy of canopy nitrogen content and hence crop
385 productivity. Yield variability was better captured by GDVI than NDVI for maize yield estimation in Kenya
386 (Burke and Lobell, 2017; Jin et al., 2019).

387 The 5 to 15 days periods starting around 45 days after emergence and ending around 80 days after
388 emergence maximized the accuracy of yield estimates (Fig 3b). For the short-cycle (90 days) *souna* millet
389 grown in the study area, it extends over the end of the panicle initiation and the grain filling phase. Millet
390 growth, grain number per unit area and grain filling are particularly sensitive to water, thermal and
391 nitrogen stresses during these periods. Leroux et al. (2016), Maselli et al. (2000) and Rasmussen (1992)
392 also reported that millet yield estimates accuracy was maximized when considering flowering and grain
393 filling periods in Niger and Burkina Faso.

394 Spatial variability in estimated pearl millet yield was large for our study area. Yield in half of the patches
395 could be increased by more than 60% to close the gap with the highest attainable yield observed in the
396 landscape (Fig 5). The highest attainable yield (i.e. the 95th percentile) was 1912 kg/ha, similar to the one

observed by Affholder et al. (2013) in the same region. Remote sensing based yield estimates evidenced a clear spatial pattern in millet yield variability: greater yields were found close to the main village. This finding is consistent with the ring cultivation scheme often found across Sub-saharan Africa: farmers allocate more manure and labour to 'home fields' causing soil fertility to decrease from homesteads to bush fields (Affholder, 1995; Manlay et al., 2004; Prudencio, 1993; Tittonell et al., 2013).

4.2 Soil fertility drives yield spatial variability in parklands

Spatial variability of crop yields in Sahelian smallholder farming systems is caused by variability in environmental and management factors across farms. Quantifying and explaining yield spatial variability can inform improvements in agricultural practices toward an increase in crop yield.

Yield varied largely over short distances in our study area. By combining remote sensing and machine learning, we unravelled the contribution of fine-scale variation in biophysical and management-related factors to explain yield spatial variability. Agronomic variables (*i.e.* soil nutrient and nutrient stress) prevailed over landscape variables (Fig 6b and Fig 6c). Low mineral fertilizer inputs use and low soil fertility are major crop yield limiting factors across sub-Saharan Africa (*e.g.* Beza et al., 2017; Mueller et al., 2012) and more generally in family farms across the tropics (Affholder et al., 2013). Mineral and/or organic fertilizer was applied on half of the monitored field of our study only, with a maximum input of 65 kgN/ha, *i.e.* a rather low amount compared with the amount of N required to close cereal yield gaps in the region (ten Berge et al., 2019). Soil organic nitrogen and total phosphorous content were the most important drivers of yield variability. Without mineral fertilizer inputs, organic nitrogen strongly drives the amount of mineral N available for crop growth. Total phosphorus is related to available P for which sub-optimal values can undermine nitrogen use efficiency (Tounkara et al., 2020). Overall, our remote sensing-based study corroborates conclusions of current knowledge on sustainable intensification in sub-Saharan Africa. Integrated soil fertility management, *i.e.* optimal and efficient use of organic and mineral fertilizer, could improve crop productivity (Vanlauwe et al., 2015). However, in complex parkland, the boosting effect of fertilizer on crop productivity can be offset depending on tree-crop combinations (Sida et al., 2019).

Maintenance and regeneration of agroforestry parklands can also be a relevant entry point for integrated soil fertility management and sustainable intensification.

4.3 Trees no longer benefit to crops above 40% woody cover in surrounding landscape

Our results showed that landscape woody cover (*i.e.* the share of field area covered by tree crown projection) in the surrounding landscape of patches was an important driver of yield variability (Fig 6b). Parklands are outstandingly anisotropic landscapes, and hold a large diversity of trees with specific densities. Processes occurring outside fields are likely to impact within-fields crop yield (Luedeling et al., 2016). Impacts of landscape-scale woody cover on regulating services in West Africa include pests biological control (Soti et al., 2019), water flow regulation (Smith et al., 1997), wind erosion control (Leenders et al., 2007) and carbon storage (Takimoto et al., 2008). *F.albida* was found to be the only species positively impacting cereals in diverse parklands across West Africa Bayala et al. (2012). *F.albida* can substantially improve nitrogen, phosphorous and soil organic carbon balances in agrosystems (*e.g.* through deep capture and improved nutrient cycling) particularly in low-fertility and below-average rainfall conditions (Sileshi, 2016; Sinare and Gordon, 2015). In Northern Ethiopia, total nitrogen and available phosphorus increased with *F.albida* cover (Hadgu et al., 2009). Using remote sensing to map woody shrub cover, Lufafa et al. (2008) evidenced an increase in above ground biomass carbon in Senegal concomitant with woody cover. Our analysis suggested that a 30-40% landscape woody cover maximizes the positive impact of trees on crops (Fig 6d). Above 40% and depending on tree species, it is likely that trees compete more strongly with crop for nutrient, water and light. For instance, the positive tree-scale effects of *F.albida* (*e.g.* Kho et al., 2001; Louppe et al., 1996; Sida et al., 2018) can be mitigated at landscape scale depending of the share of *F.albida,* the number of trees and the diversity of trees in the field: Hadgu et al. (2009) have shown that for *Eucalyptus camaldulensis* parklands in Ethiopia, *F.albida*'s positive impact on barley yield were offset by the nutrient and water demand of *E.camaldulensis*.

Our analysis points to the need to strengthen remote sensing-based models with information related to tree species. In West Africa, most studies conducted on individual trees mapping using very high spatial resolution images focused on tree density and woody cover (Herrmann et al., 2013; Karlson et al., 2014;

448 Schnell et al., 2015). Despite the launch of new satellites at a spatial and spectral resolution suited for tree
449 species mapping (*e.g.* Worldview-2/3), few studies were conducted in the African context so far. The study
450 of Karlson et al. (2016) in Burkina Faso and Madonsela et al. (2017) in South-Africa are useful exceptions.
451 Mapping tree species in the diverse West African parklands requires multi-seasonal images to discriminate
452 tree species according to their phenological development. New satellite images at high spatial (5-m),
453 spectral (12 bands) and temporal (2-days) resolutions (*e.g.* Venμs) open new avenues for tree species
454 mapping in complex agricultural landscape. Additional improvements would entail the strengthening of
455 individual trees identification. We used a threshold approach based on PlanetScope NDVI images. With the
456 spatial resolution of PlanetScope images (3-m) and the parkland density observed in some fields (> 30
457 trees/ha), the number of trees was underestimated in some cases due to the identification of clusters of
458 trees rather than individual trees. An approach combining very high spatial resolution images (*e.g.*
459 Worldview or Pleiades) with an object-based image analysis could help to improve tree crown delineation
460 (Karlson et al., 2014)

461 **4.4 Implication for agricultural policies in West Africa**

462 Specific policies aiming at improving cash availability (*e.g.* with subsidized short-term credit or subsidized
463 fertilizers) and reducing risk exposure (*e.g.* with drought insurance) would incentivize farmers to
464 adequately fertilize their fields, which could contribute to poverty reduction in the Senegalese groundnut
465 basin (Ricome et al. 2017). Our study shows that such policies could also target tree density management
466 as it also contributes to millet productivity. For example, the promotion of farmer managed natural tree
467 regeneration (Haglund et al., 2011) with trainings and capacity building could deserve more attention.
468 However, increasing landscape woody cover above 40% seems to provide limited additional benefits to
469 millet productivity, indicating that areas with woody cover below this threshold should be prioritized. This
470 study was conducted in a small *F.albida* parkland in central Senegal. The robustness of our approach needs
471 to be tested in larger areas across sub-Saharan Africa with more diverse and contrasting household
472 resource endowment, occurrence of pest and diseases, tree density and diversity, and landscape woody
473 cover. Despite this limitation, our study shows that high-resolution remote sensing images can help
474 understand the drivers of yield spatial variability over fine spatial scale . We believe that that further

developing this approach in combination with socio-economic information could contribute to frame location-specific recommendations for soil fertility and biodiversity management options in agroforestry parklands.

5 Conclusion

Agroforestry attracted the attention of policies as an entry point to address climate change and food security challenges (IPCC, 2019). Reliable assessment of crop yields under parkland systems are urgently needed to inform global debates and foster local policy interventions. Few studies have tackled the challenge to assess the effects of agroforestry parklands on crops production beyond tree scale. By adopting landscape scale as an entry point and using cutting-edge remote sensing images, modelling approaches and ground observation in the Groundnut Basin of Senegal, our study adds to the existing literature that points to the relevance of agroforestry in addressing societal and environmental challenges in Africa.

We proposed a remote sensing-based model that allowed accurate crop yield estimations in agroforestry parklands, applied to a case study of Central Senegal. The model integrated variables related to parkland structure, a current common omission when dealing with yield estimation in smallholder agriculture with remote sensing. The model explained 70% of observed millet yield variability. The yield map generated by this model showed that half of fields had yields that could be increased by more than 60%. Soil Organic N , total P and woody cover in the surrounding landscape of fields were identified as the most important drivers of millet yield spatial variability. Interestingly, there was a landscape woody cover threshold above which crops no longer benefit from the presence of trees. Our study confirms that soil fertility improvement should be the core focus of policies aiming at promoting sustainable intensification of millet production in the region. But we also show that parkland maintenance and regeneration should not be overlooked. Tree species mapping to account for the full complexity of agroforestry parkland systems at landscape scale is a critical issue that now has to be addressed by the remote sensing community.

Acknowledgement : This study was supported by the LYSA project (DAR-TOSCA 4800001089) funded by the French Space Agency (CNES), the SERENA project funded by the Cirad-INRA metaprogramme GloFoodS and the SIMCo project (agreement number 201403286-10) funded by the Feed The Future Sustainable Innovation Lab (SIIL) through the USAID AID-OOA-L-14-00006. Sentinel-2 data were obtained from the Theia processing

center at CNES (https://theia.cnes.fr/atdistrib/rocket). We acknowledge Planet's Ambassador Program for the access to their Planet and RapidEye images. The authors are very thankful to PhD students (Sophie Djiba, Adama Tounkara and Medoune Mbengue) for sharing their agronomical data in 2017, to Robert Diatta for his help during the field survey in 2018, to Idrissa Faye and its family for its valuable assistance and to the two anonymous reviewers for useful suggestions on earlier version of the manuscript.

.

Reference

Affholder, F., 1997. Empirically modelling the interaction between intensification and climatic risk in semiarid regions. F. Crop. Res. 52, 79–93. doi:10.1016/S0378-4290(96)03453-3

Affholder, F., 1995. Effect of organic matter input on the water balance and yield of millet under tropical dryland condition. F. Crop. Res. 41, 109–121. doi:10.1016/0378-4290(94)00115-S

Affholder, F., Poeydebat, C., Corbeels, M., Scopel, E., Tittonell, P., 2013. The yield gap of major food crops in family agriculture in the tropics: Assessment and analysis through field surveys and modelling. F. Crop. Res. 143, 106–118. doi:10.1016/j.fcr.2012.10.021

Baudron, F., Schultner, J., Duriaux, J.Y., Gergel, S.E., Sunderland, T., 2019. Agriculturally productive yet biodiverse: human benefits and conservation values along a forest-agriculture gradient in Southern Ethiopia. Landsc. Ecol. 34, 341–356. doi:10.1007/s10980-019-00770-6

Bayala, J., Sanou, J., Teklehaimanot, Z., Ouédraogo, S.J., 2014. Parklands for buffering climate risk and sustaining agricultural production in the Sahel of West Africa. Curr. Opin. Environ. Sustain. 6, 28–34. doi:10.1016/J.COSUST.2013.10.004

Bayala, J., Sanou, J., Teklehaimanot, Z., Ouedraogo, S.J., Kalinganire, A., Coe, R., Noordwijk, M. va., 2015. Advances in knowledge of processes in soil–tree–crop interactions in parkland systems in the West African Sahel: A review. Agric. Ecosyst. Environ. 205, 25–35. doi:10.1016/J.AGEE.2015.02.018

Bayala, J., Sileshi, G.W., Coe, R., Kalinganire, A., Tchoundjeu, Z., Sinclair, F., Garrity, D., 2012. Cereal yield response to conservation agriculture practices in drylands of West Africa: A quantitative synthesis. J. Arid Environ. doi:10.1016/j.jaridenv.2011.10.011

Beza, E., Silva, J.V., Kooistra, L., 2017. Review of yield gap explaining factors and opportunities for alternative data collection approaches. Eur. J. Agron. 82, 206–222. doi:10.1016/j.eja.2016.06.016

Boffa, J.-M., 1999. Agroforestry Parklands in Sub-Saharan Africa (No. 34), FAO Conservation Guide. Rome, Italy.

Breiman, 2001. Random Forest. Mach. Learn. 45, 5–32.

Burke, M., Lobell, D.B., 2017. Satellite-based assessment of yield variation and its determinants in smallholder African systems. Proc. Natl. Acad. Sci. U. S. A. 114, 2189–2194. doi:10.1073/pnas.1616919114

Daughtry, C.S.., Walthall, C.., Kim, M.., de Colstoun, E.B., McMurtrey, J.., 2000. Estimating Corn Leaf Chlorophyll Concentration from Leaf and Canopy Reflectance. Remote Sens. Environ. 74, 229–239. doi:10.1016/S0034-4257(00)00113-9

Delaunay, V., Douillot, L., Diallo, A., Dione, D., Trape, J.F., Medianikov, O., Raoult, D., Sokhna, C., 2013. Food. Int. J. Epidemiol. 42, 1002–1011. doi:10.1093/ije/dyt100

Duncan, J.M.A., Dash, J., Atkinson, P.M., 2015. The potential of satellite-observed crop phenology to enhance yield gap assessments in smallholder landscapes. Front. Environ. Sci. 3, 1–16. doi:10.3389/fenvs.2015.00056

Duriaux Chavarría, J.Y., Baudron, F., Sunderland, T., 2018. Retaining forests within agricultural landscapes as a pathway to sustainable intensification: Evidence from Southern Ethiopia. Agric. Ecosyst. Environ. 263, 41–52. doi:10.1016/J.AGEE.2018.04.020

Eilers, P.H.C., 2003. A Perfect Smoother. doi:10.1021/AC034173T

Fischler, M.A., Bolles, R.C., 1981. Random sample consensus: a paradigm for model fitting with applications to image analysis and automated cartography. Commun. s ACM 24, 381–395.

Forkel, M., Carvalhais, N., Verbesselt, J., Mahecha, M., Neigh, C., Reichstein, M., 2013. Trend Change Detection in NDVI Time Series: Effects of Inter-Annual Variability and Methodology. Remote Sens. 5, 2113–2144.

551 doi:10.3390/rs5052113

552 Friedman, J.H., 2001. Greedy function approximation: A gradient boosting machine. Ann. Stat. 29, 1189–1232.

553 Friedman, J.H., Meulman, J.J., 2003. Multiple additive regression trees with application in epidemiology. Stat. Med. 22,
554 1365–1381.

555 Fritz, S., See, L., Mccallum, I. a N., You, L., Bun, A., Moltchanova, E., Duerauer, M., Albrecht, F., Schill, C., Perger, C.,
556 Havlik, P., Mosnier, A., Thornton, P., Wood-sichra, U., Herrero, M., Becker-Reshef, I., 2015. Mapping global
557 cropland and field size. Glob. Chang. Biol. 21, 1–13. doi:10.1111/gcb.12838

558 Gitelson, A.A., Viña, A., Ciganda, V., Rundquist, D.C., Arkebauer, T.J., 2005. Remote estimation of canopy chlorophyll
559 content in crops. Geophys. Res. Lett. 32, L08403. doi:10.1029/2005GL022688

560 Greenwell, B., Boehmke, B., Cunningham, J., GBM Developers, ., 2019. gbm: Generalized Boosted Regression Models.

561 Hadgu, K.M., Kooistra, L., Rossing, W.A.H., van Bruggen, A.H.C., 2009. Assessing the effect of Faidherbia albida
562 based land use systems on barley yield at field and regional scale in the highlands of Tigray, Northern Ethiopia.
563 Food Secur. 1, 337–350. doi:10.1007/s12571-009-0030-2

564 Haglund, E., Ndjeunga, J., Snook, L., Pasternak, D., 2011. Dry land tree management for improved household
565 livelihoods: farmer managed natural regeneration in Niger. J. Environ. Manage. 92, 1696–1705.
566 doi:10.1016/j.jenvman.2011.01.027

567 Hagolle, O., Huc, M., Pascual, D.V., Dedieu, G., 2010. A multi-temporal method for cloud detection, applied to
568 FORMOSAT-2, VENμS, LANDSAT and SENTINEL-2 images. Remote Sens. Environ.
569 doi:10.1016/j.rse.2010.03.002

570 Haralick, R.., Shanmugan, K., 1973. Textural features for image classification. IEEE Trans. Syst. Man Cybern. 6, 610–
571 621.

572 Hengl, T., Heuvelink, G.B.M., Kempen, B., Leenaars, J.G.B., Walsh, M.G., Shepherd, K.D., Sila, A., MacMillan, R.A., De
573 Jesus, J.M., Tamene, L., Tondoh, J.E., 2015. Mapping soil properties of Africa at 250 m resolution: Random
574 forests significantly improve current predictions. PLoS One 10. doi:10.1371/journal.pone.0125814

575 Hengl, T., Leenaars, J.G.B., Shepherd, K.D., Walsh, M.G., Heuvelink, G.B.M., Mamo, T., Tilahun, H., Berkhout, E.,
576 Cooper, M., Fegraus, E., Wheeler, I., Kwabena, N.A., 2017. Soil nutrient maps of Sub-Saharan Africa: assessment
577 of soil nutrient content at 250 m spatial resolution using machine learning. Nutr. Cycl. Agroecosystems 109, 77–
578 102. doi:10.1007/s10705-017-9870-x

579 Herrmann, S., Wickhorst, A., Marsh, S., 2013. Estimation of Tree Cover in an Agricultural Parkland of Senegal Using
580 Rule-Based Regression Tree Modeling. Remote Sens. 5, 4900–4918. doi:10.3390/rs5104900

581 IPCC, 2019. Summary for Policymakers, in: Climate Change and Land: An IPCC Special Report on Climate Change,
582 Desertification, Land Degradation, Sustainable Land Management, Food Security, and Greenhouse Gas Fluxes
583 in Terrestrial Ecosystems. p. In press.

584 Jain, M., Singh, B., Srivastava, A.K., Malik, R.K., McDonald, A., Lobell, D.B., 2017. Using satellite data to identify the
585 causes of and potential solutions for yield gaps in India's Wheat Belt. Environ. Res. Lett. 12, 094011.
586 doi:10.1088/1748-9326/aa8228

587 Jin, Z., Azzari, G., Burke, M., Aston, S., Lobell, D., 2017. Mapping Smallholder Yield Heterogeneity at Multiple Scales in
588 Eastern Africa. Remote Sens. 9, 931. doi:10.3390/rs9090931

589 Jin, Z., Azzari, G., You, C., Di Tommaso, S., Aston, S., Burke, M., Lobell, D.B., 2019. Smallholder maize area and yield
590 mapping at national scales with Google Earth Engine. Remote Sens. Environ. 228, 115–128.
591 doi:10.1016/J.RSE.2019.04.016

592 Karlson, M., Ostwald, M., Reese, H., Bazié, H.R., Tankoano, B., 2016. Assessing the potential of multi-seasonal
593 WorldView-2 imagery for mapping West African agroforestry tree species. Int. J. Appl. Earth Obs. Geoinf. 50,
594 80–88. doi:10.1016/j.jag.2016.03.004

595 Karlson, M., Reese, H., Ostwald, M., 2014. Tree Crown Mapping in Managed Woodlands (Parklands) of Semi-Arid West
596 Africa Using WorldView-2 Imagery and Geographic Object Based Image Analysis. Sensors 14, 22643–22669.
597 doi:10.3390/s141222643

598 Kho, R.M., Yacouba, B., Yayé, M., Katkoré, B., Moussa, A., Iktam, A., Mayaki, A., 2001. Separating the effects of trees

599 on crops: the case of Faidherbia albida and millet in Niger. Agrofor. Syst. 52, 219–238.
600 doi:10.1023/A:1011820412140

601 Lalou, R., Sultan, B., Muller, B., Ndonky, A., 2019. Does climate opportunity facilitate smallholder farmers' adaptive
602 capacity in the Sahel? Palgrave Commun. 5, 81. doi:10.1057/s41599-019-0288-8

603 Lambert, M.-J., Traoré, P.S., Blaes, X., Baret, P., Defourny, P., 2018. Estimating smallholder crops production at village
604 level from Sentinel-2 time series in Mali's cotton belt. Remote Sens. Environ. 216.
605 doi:https://doi.org/10.1016/j.rse.2018.06.036

606 Leenders, J.K., Boxel, J.H. va., Sterk, G., 2007. The effect of single vegetation elements on wind speed and sediment
607 transport in the Sahelian zone of Burkina Faso. Earth Surf. Process. Landforms 32, 1454–1474.
608 doi:10.1002/esp.1452

609 Lericollais, A. (1940-. . .)., 1999. Paysans sereer dynamiques agraires et mobilités au Sénégal. Institut de recherche
610 pour le développement (IRD).

611 Leroux, L., Baron, C., Zoungrana, B., Traoré, S.B., Lo Seen, D., Bégué, A., 2016. Crop Monitoring Using Vegetation And
612 Thermal Indices For Yield Estimates: Case Study Of A Rainfed Cereal In Semi-Arid West Africa. IEEE J. Sel. Top.
613 Appl. Earth Obs. Remote Sens. 9, 347–362. doi:10.1109/JSTARS.2015.2501343

614 Leroux, L., Castets, M., Baron, C., Escorihuela, M.J., Lo Seen, D., Bégué, A., 2019. Maize yield estimation in West
615 Africa from crop processes-induced combination of multi-domain remote sensing indices. Eur. J. Agron. 108,
616 11–26.

617 Lobell, D.B., Azzari, G., 2017. Satellite detection of rising maize yield heterogeneity in the U.S. Midwest. Environ. Res.
618 Lett. 12, 014014. doi:10.1088/1748-9326/aa5371

619 Lobell, D.B., Di Tommaso, S., You, C., Yacoubou Djima, I., Burke, M., Kilic, T., 2019. Sight for Sorghums: Comparisons
620 of Satellite- and Ground-Based Sorghum Yield Estimates in Mali. Remote Sens. 12, 100. doi:10.3390/rs12010100

621 Louppe, D., N'Dour, B., Samba, S.A.N., 1996. Influence de Faidherbia albida sur l'arachide et le mil au Sénégal, in: Les
622 Parcs à Faidherbia" (Acacia Albida Parklands), Cahiers Scientifiques Du Cirad-Forêt N°12. CIRAD, Montpellier,
623 France, pp. 123–139.

624 Löw, F., Biradar, C., Fliemann, E., Lamers, J.P.A., Conrad, C., 2017. Assessing gaps in irrigated agricultural productivity
625 through satellite earth observations—A case study of the Fergana Valley, Central Asia. Int. J. Appl. Earth Obs.
626 Geoinf. 59, 118–134.

627 Luedeling, E., Smethurst, P.J., Baudron, F., Bayala, J., Huth, N.I., van Noordwijk, M., Ong, C.K., Mulia, R., Lusiana, B.,
628 Muthuri, C., Sinclair, F.L., 2016. Field-scale modeling of tree–crop interactions: Challenges and development
629 needs. Agric. Syst. 142, 51–69. doi:10.1016/J.AGSY.2015.11.005

630 Lufafa, A., Bolte, J., Wright, D., Khouma, M., Diedhiou, I., Dick, R.P., Kizito, F., Dossa, E., Noller, J.S., 2008. Regional
631 carbon stocks and dynamics in native woody shrub communities of Senegal's Peanut Basin. Agric. Ecosyst.
632 Environ. 128, 1–11. doi:10.1016/J.AGEE.2008.04.013

633 Madonsela, S., Cho, M.A., Mathieu, R., Mutanga, O., Ramoelo, A., Kaszta, Ż., de Kerchove, R.V., Wolff, E., 2017. Multi-
634 phenology WorldView-2 imagery improves remote sensing of savannah tree species. Int. J. Appl. Earth Obs.
635 Geoinf. 58, 65–73. doi:10.1016/j.jag.2017.01.018

636 Manlay, R.J., Ickowicz, A., Masse, D., Floret, C., Richard, D., Feller, C., 2004. Spatial carbon, nitrogen and phosphorus
637 budget of a village in the West African savanna - I. Element pools and structure of a mixed-farming system.
638 Agric. Syst. 79, 55–81. doi:10.1016/S0308-521X(03)00053-2

639 Maselli, F., Romanelli, S., Bottai, L., Maracchi, G., 2000. Processing of GAC NDVI data for yield forecasting in the
640 Sahelian region. Int. J. Remote Sens. 21, 3509–3523. doi:10.1080/014311600750037525

641 Merzlyak, M.N., Gitelson, A.A., Chivkunova, O.B., Rakitin, V.Y., 1999. Non-destructive optical detection of pigment
642 changes during leaf senescence and fruit ripening. Physiol. Plant. 106, 135–141. doi:10.1034/j.1399-
643 3054.1999.106119.x

644 Mkhabela, M.S., Mkhabela, M.S., Mashinini, N.N., 2005. Early maize yield forecasting in the four agro-ecological
645 regions of Swaziland using NDVI data derived from NOAA's-AVHRR. Agric. For. Meteorol. 129, 1–9.
646 doi:10.1016/J.AGRFORMET.2004.12.006

647 Mueller, M.D., Gerber, J.S., Johnston, M., Ray, D.K., Ramankutty, N., Foley, J.A., 2012. Closing yield gaps through

nutrient and water management. Nature, UK 490, 254–257.

Nair, P., 1993. An introduction to agroforestry, Springer S. ed. Dordrecht, The Netherlands.

Ndao, B., Leroux, L., Diouf, A.A., Soti, V., Sambou, B., 2019. A remote sensing based approach for optimizing sampling strategies in tree monitoring and agroforestry systems mapping, in: Dupraz, C., Gosme, M., Lawson, G. (Eds.), Agroforestry. CIRAD, INRA, World Agroforestry, Agropolis International, MUSE, Montpellier, France, p. 563.

Ndao, B., Leroux, L., Diouf, A.A., Soti, V., Sambou, B., 2018. A remote sensing based approach for optimizing sampling strategies in crop monitoring and crop yield estimation studies, in: Wade, S. (Ed.), Earth Observations and Geospatial Science in Service of Sustainable Development Goals : 12th International Conference of the African Association of Remote Sensing and the Environment. Springer, Muinzenburg, South Africa, pp. 25–36. doi:https://doi.org/10.1007/978-3-030-16016-6_3

Oerke, E.C., 2006. Crop losses to pests. J. Agric. Sci. doi:10.1017/S0021859605005708

Peltier, R., 1996. Les Parcs à Faidherbia" (Acacia albida Parklands), Cahiers scientifiques du Cirad-Forêt n°12. CIRAD, Montpellier, France.

Planet-Team, 2018. Planet Imagery products specifications.

Prudencio, C.Y., 1993. Ring management of soils and crops in the west African semi-arid tropics: The case of the mossi farming system in Burkina Faso. Agric. Ecosyst. Environ. 47, 237–264. doi:10.1016/0167-8809(93)90125-9

Rasmussen, M.S., 1992. Assessment of millet yields and production in northern Burkina Faso using integrated NDVI from the AVHRR. Int. J. Remote Sens. 13, 3431–3442. doi:10.1080/01431169208904132

Reed, J., Van Vianen, J., Deakin, E.L., Barlow, J., Sunderland, T., 2016. Integrated landscape approaches to managing social and environmental issues in the tropics: learning from the past to guide the future. Glob. Chang. Biol. 22, 2540–2554. doi:10.1111/gcb.13284

Ricome, A., Affholder, F., Gérard, F., Muller, B., Poeydebat, C., Quirion, P., Sall, M., 2017. Are subsidies to weather-index insurance the best use of public funds? A bio-economic farm model applied to the Senegalese groundnut basin. Agric. Syst. 156, 149–176. doi:10.1016/j.agsy.2017.05.015

Sanou, J., Bayala, J., Teklehaimanot, Z., Bazié, P., 2012. Effect of shading by baobab (Adansonia digitata) and néré (Parkia biglobosa) on yields of millet (Pennisetum glaucum) and taro (Colocasia esculenta) in parkland systems in Burkina Faso, West Africa. Agrofor. Syst. 85, 431–441. doi:10.1007/s10457-011-9405-4

Schnell, S., Kleinn, C., Ståhl, G., 2015. Monitoring trees outside forests: a review. Environ. Monit. Assess. 187, 600. doi:10.1007/s10661-015-4817-7

Sida, T.S., Baudron, F., Kim, H., Giller, K.E., 2018. Climate-smart agroforestry: Faidherbia albida trees buffer wheat against climatic extremes in the Central Rift Valley of Ethiopia. Agric. For. Meteorol. 248, 339–347. doi:10.1016/J.AGRFORMET.2017.10.013

Sida, T.S., Baudron, F., Ndoli, A., Tirfessa, D., Giller, K.E., 2019. Should fertilizer recommendations be adapted to parkland agroforestry systems? Case studies from Ethiopia and Rwanda. Plant Soil 1–16. doi:10.1007/s11104-019-04271-y

Sileshi, G.W., 2016. The magnitude and spatial extent of influence of Faidherbia albida trees on soil properties and primary productivity in drylands. J. Arid Environ. 132, 1–14. doi:10.1016/J.JARIDENV.2016.03.002

Sinare, H., Gordon, L.J., 2015. Ecosystem services from woody vegetation on agricultural lands in Sudano-Sahelian West Africa. Agric. Ecosyst. Environ. 200, 186–199. doi:10.1016/j.agee.2014.11.009

Smith, D.M., Jarvis, P.G., Odongo, J.C.., 1997. Sources of water used by trees and millet in Sahelian windbreak systems. J. Hydrol. 198, 140–153. doi:10.1016/S0022-1694(96)03311-2

Soti, V., Thiaw, I., Debaly, M.Z., Sow, A., Diaw, M., Fofana, S., Diakhate, M., Thiaw, C., Brévault, T., 2019. Effect of landscape diversity and crop management on the control of the millet head miner, Heliocheilus albipunctella (Lepidoptera: Noctuidae) by natural enemies. Biol. Control 129, 115–122. doi:10.1016/j.biocontrol.2018.10.006

Takimoto, A., Nair, P.K.R., Nair, V.D., 2008. Carbon stock and sequestration potential of traditional and improved agroforestry systems in the West African Sahel. Agric. Ecosyst. Environ. 125, 159–166. doi:10.1016/J.AGEE.2007.12.010

ten Berge, H.F.M., Hijbeek, R., van Loon, M.P., Rurinda, J., Tesfaye, K., Zingore, S., Craufurd, P., van Heerwaarden, J., Brentrup, F., Schröder, J.J., Boogaard, H.L., de Groot, H.L.E., van Ittersum, M.K., 2019. Maize crop nutrient input requirements for food security in sub-Saharan Africa. Glob. Food Sec. 23, 9–21. doi:10.1016/j.gfs.2019.02.001

Tittonell, P., Muriuki, A., Klapwijk, C.J., Shepherd, K.D., Coe, R., Vanlauwe, B., 2013. Soil heterogeneity and soil fertility gradients in smallholder farms of the east african highlands soil fertility & plant nutrition. Soil Sci. Soc. Am. J. 77, 525–538. doi:10.2136/sssaj2012.0250

Tounkara, A., Clermont-Dauphin, C., Affholder, F., Ndiaye, S., Masse, D., Cournac, L., 2020. Inorganic fertilizer use efficiency of millet crop varies with organic fertilizer application in rainfed agriculture on smallholdings in central Senegal. Agric. Ecosyst. Environ. 294, 106878.

United Nations, 2016. The Sustainable Development Goals Report 2016. New-York, USA. doi:https://dx.doi.org/10.18356/3405d09f-en

Vanlauwe, B., Descheemaeker, K., Giller, K.E., Huising, J., Merckx, R., Nziguheba, G., Wendt, J., Zingore, S., 2015. Integrated soil fertility management in sub-Saharan Africa: Unravelling local adaptation. SOIL 1, 491–508. doi:10.5194/soil-1-491-2015

Whitcraft, A.K., Vermote, E.F., Becker-Reshef, I., Justice, C.O., 2015. Cloud cover throughout the agricultural growing season: Impacts on passive optical earth observations. Remote Sens. Environ. 156, 438–447. doi:http://dx.doi.org/10.1016/j.rse.2014.10.009

Zhao, Y., Chen, X., Cui, Z., Lobell, D.B., 2015. Using satellite remote sensing to understand maize yield gaps in the North China Plain. F. Crop. Res. 183, 31–42. doi:10.1016/j.fcr.2015.07.004

Zomer, J.R., Trabucco, A., Coe, R., Place, F., Van Noordwijk, M., XU, J.C., 2014. Trees on farms: an update and reanalysis of agroforestry's global extent and socio-ecological characteristics (No. 179). Bogor, Indonesia. doi:10.5716/ WP14064.PDF

Figure 1

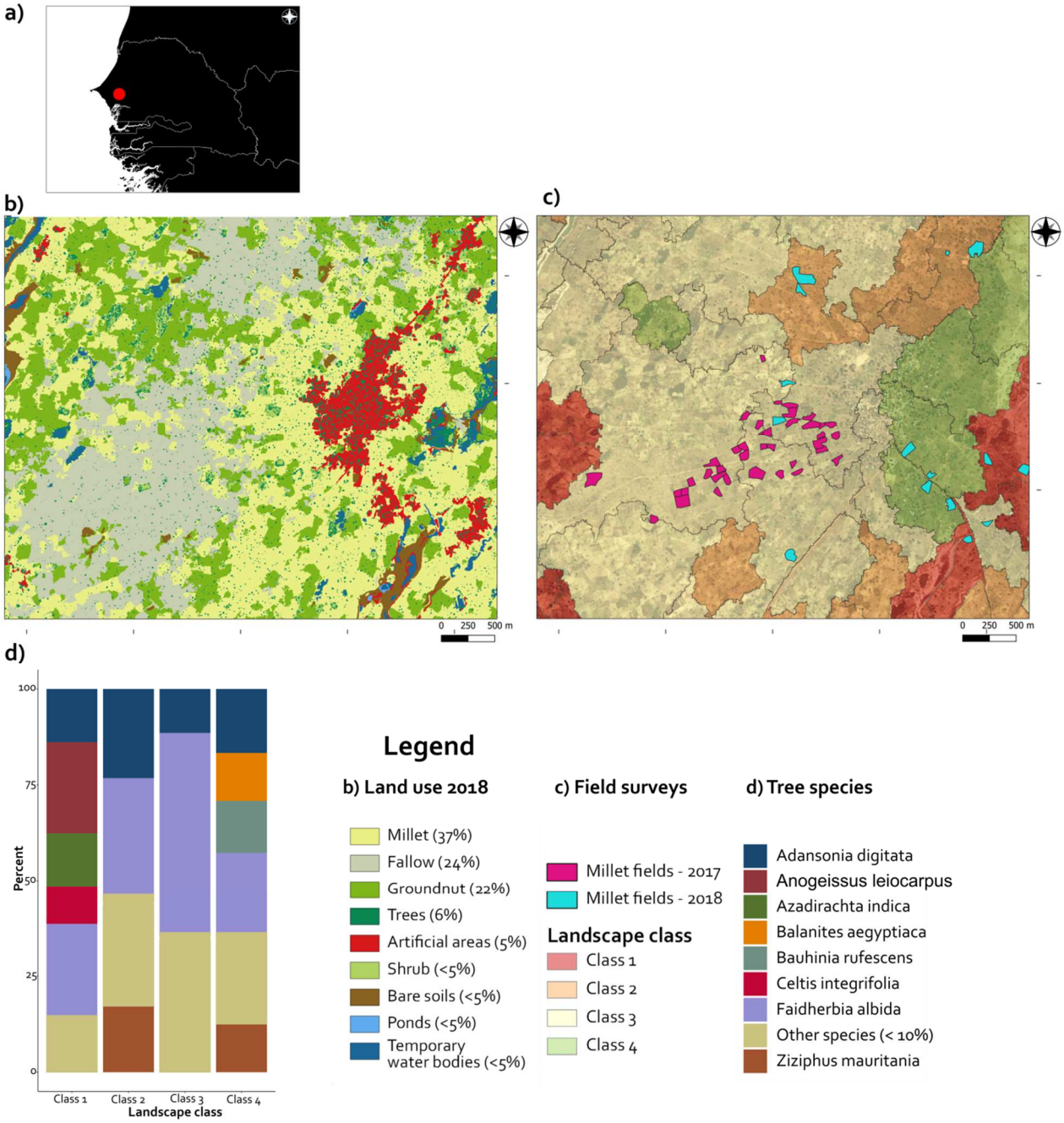

Fig 1 Main characteristics of the study site : a) location of the study area, b) main land use in 2018 (Ndao et al., 2019), c) location of farmers fields in the four landscape classes defined from a remote sensing based stratification (Ndao et al., 2018), each polygon representing a landscape class and d) tree species composition of each landscape class.

Figure 2

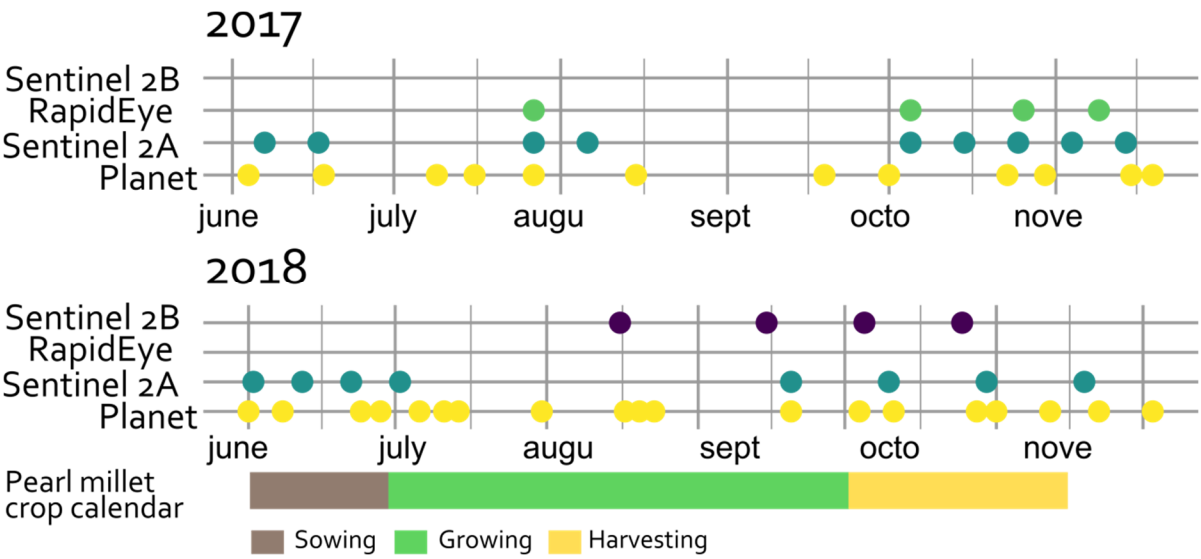

Fig 2 Acquisition dates of the satellite images with regard to pearl millet management calendar.

Figure 3

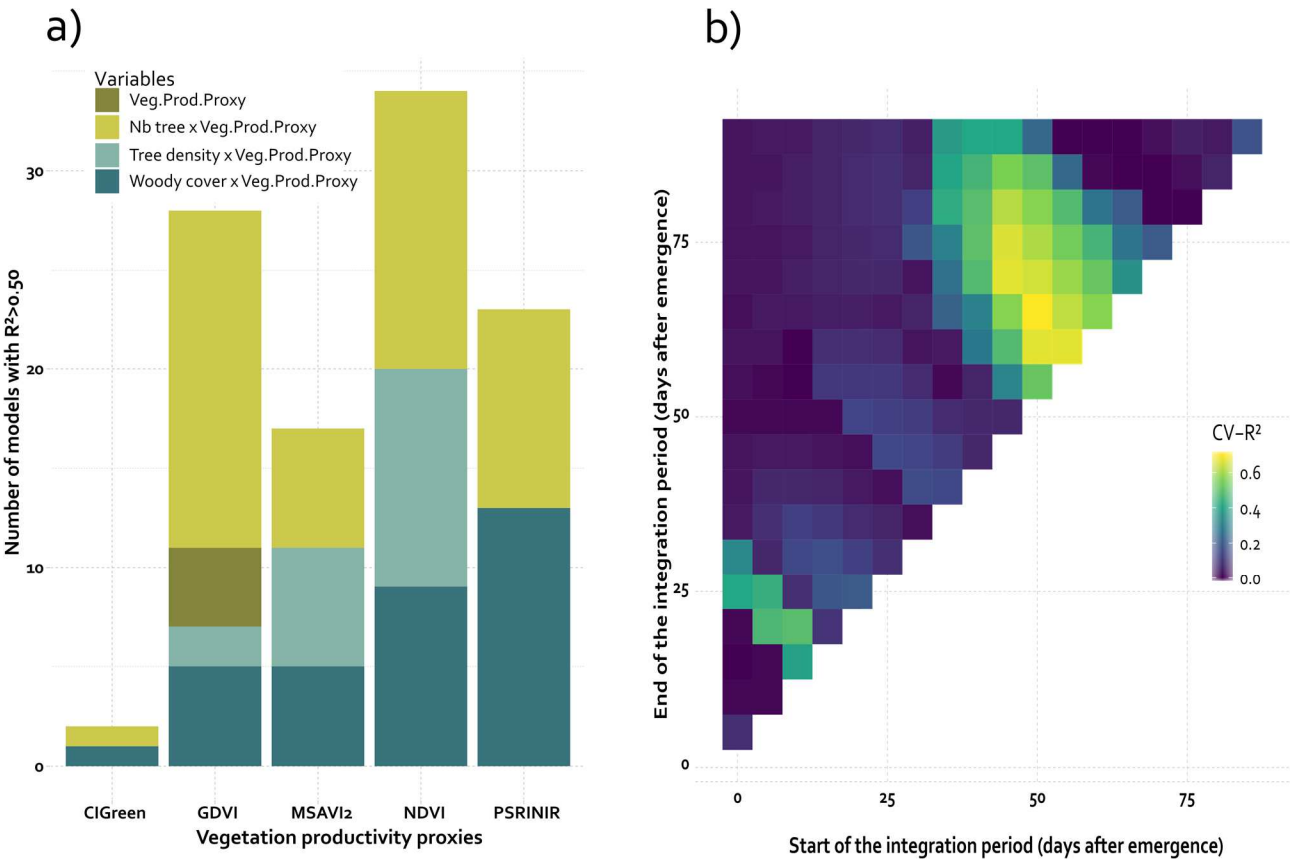

Fig 3. millet yield estimates accuracy according to (a) proxies of vegetation productivity and parkland structure when linear regression models are calibrated with and without proxies of parkland structure (i.e. number of trees, tree density and woody cover), (b) integration period for models combining GDVI and number of trees. Only models with cross-validation $R^2 > 0.50$ (p-value<0.001) are displayed in (a) (i.e. 15% of tested models). Effect of integration period on yield estimate accuracy for other vegetation productivity proxies can be found in supplementary material S4.

Figure 4

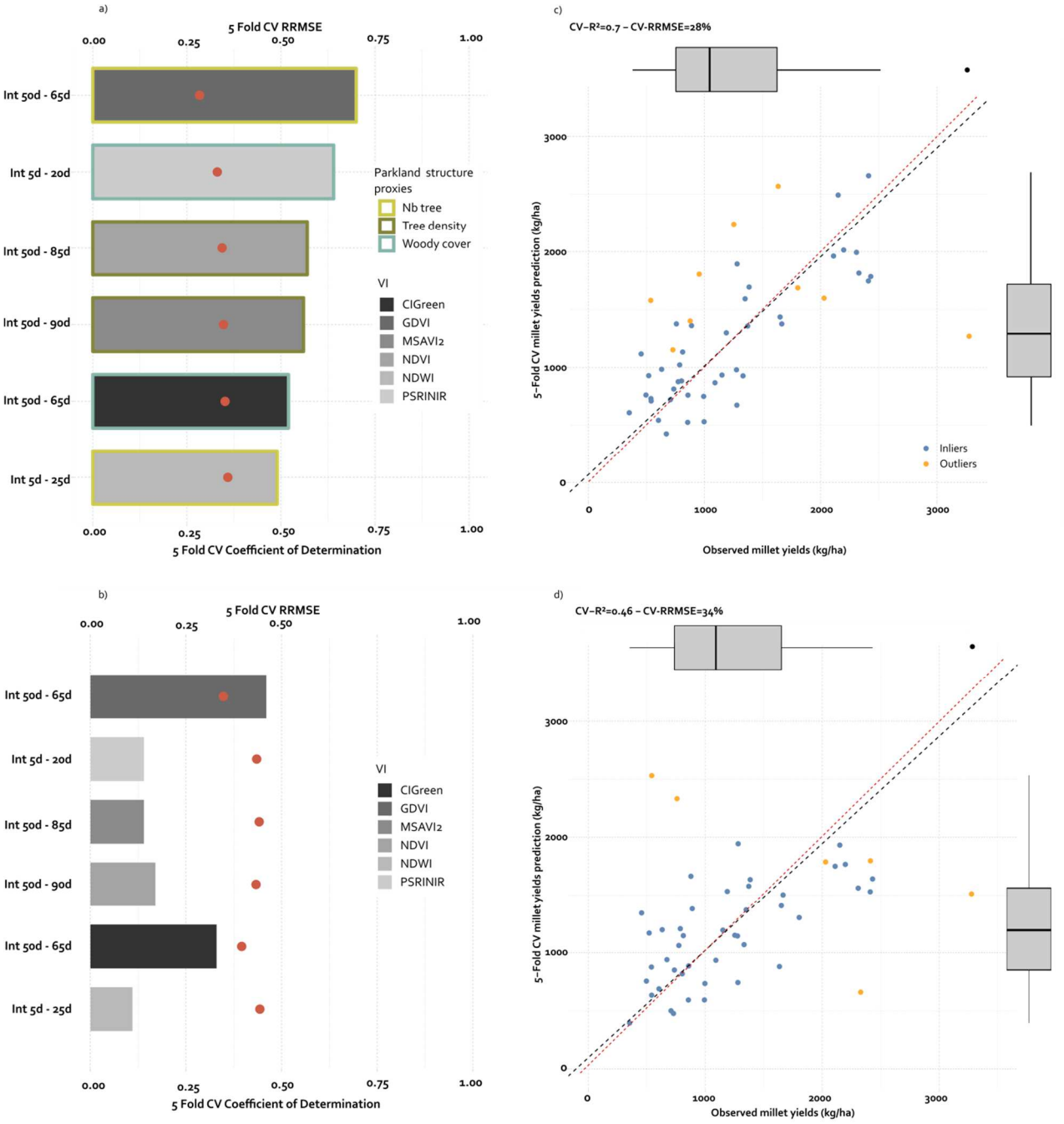

Fig 4. 5-fold cross validation R² (bars) and RRMSE (red dots) for the best model calibrated (a) with vegetation productivity proxies and parkland structure proxies and b) vegetation productivity proxy only. All models have a p-value below 0.001. c) Comparison between observed and predicted yields for the final best model (GDVI integrated of 50 to 65 days after emergence combined with the number of trees). d) Comparison between observed and predicted yields for the best model without parkland structuring information (GDVI integrated over 50 to 65 days after emergence). The red dashed line represents the 1:1 line and the black dashed line represents the regression line.

Figure 5

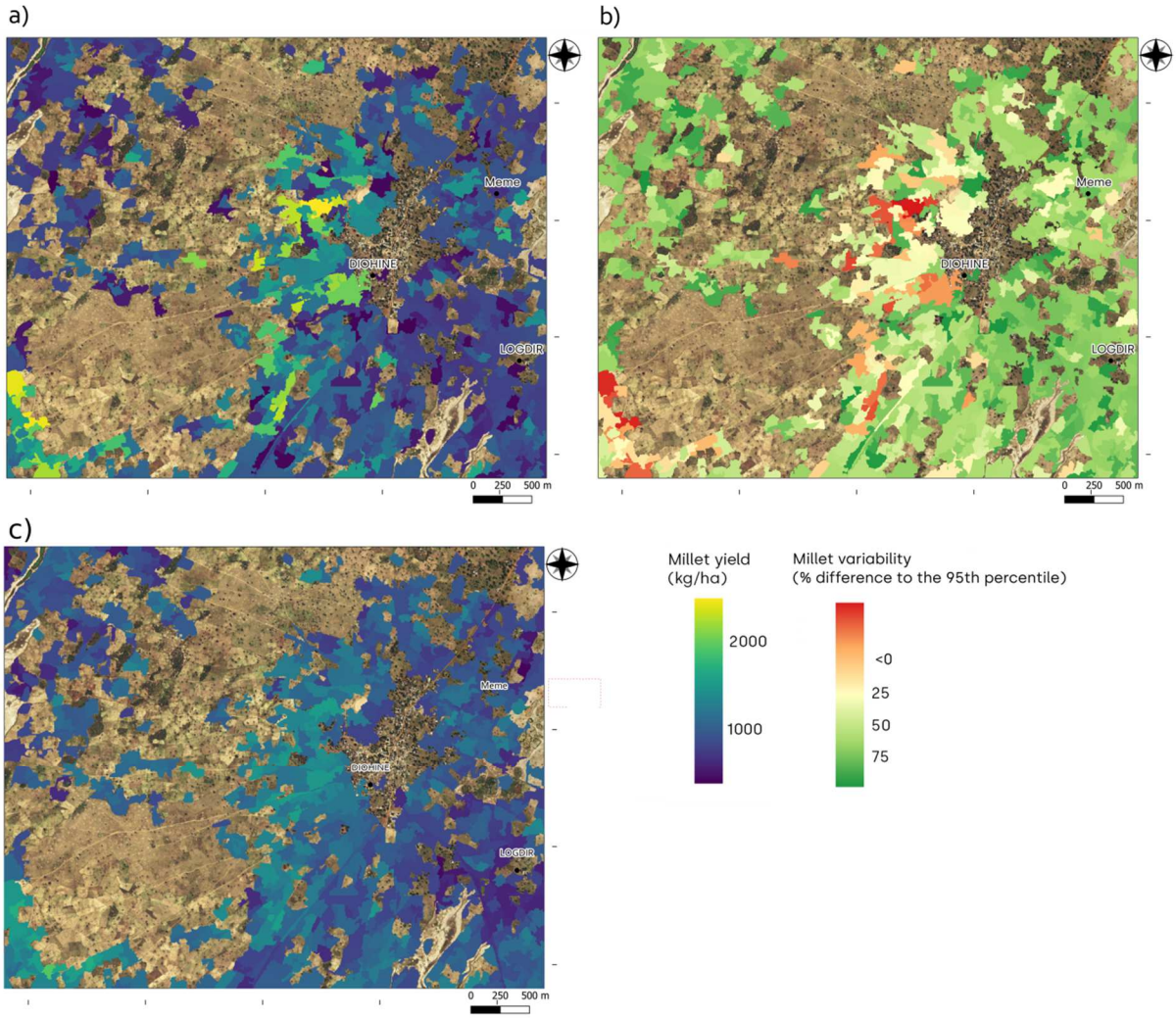

Fig 5 Millet yield over the study area at patch scale using remote sensing information. (a) Millet yield estimated for 2018 with the best model integrating parkland structure information (GDVI integrated over 50 to 65 days after emergence combined with the number of trees). (b) Corresponding variability of millet yield (% difference to the 95th percentile). (c)Millet yield estimated for 2018 using the best model without parkland structure information (GDVI integrated over 50 to 65 days after emergence).

Figure 6

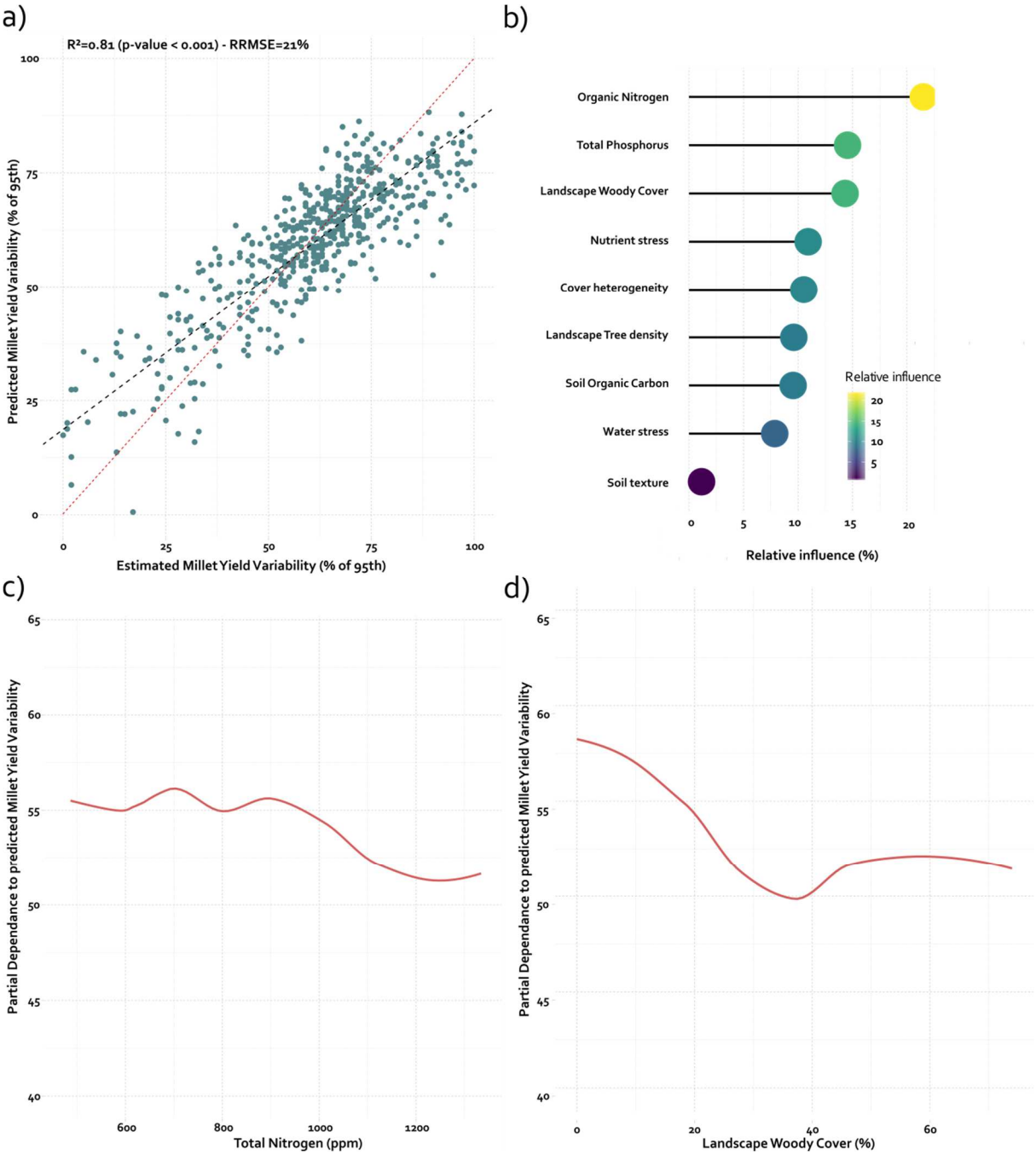

Fig 6 Effects of biophysical and management factors on spatial millet yield variability. a) Prediction performance of millet yield variability with GBM model. b) Relative influence of input variables in the GBM model, ranked by order of influence. Partial dependance plot of c) total soil organic nitrogen content and d) woody cover in surrounding landscape of millet patches. The partial dependance plot depicts the marginal effect of total nitrogen or landscape woody cover on the predicted millet yield variability (i.e. the probability of being far from the 95th percentile).

Table 1 Vegetation indices (VI) used to estimate millet yield: NDVI (Normalized Difference Vegetation Index), GDVI (Green Difference Vegetation Index), MSAVI2 (Modified Soil Adjusted Vegetation Index), PSRINIR (Plant Senescence Reflectance Index -NIR), NDWI (Normalized Difference Water Index) and CIGreen (Green Chlorophylle Index). P: PlanetScope, S: Sentinel-2 and R: RapidEye. NIR, R, G and SWIR stand respectively for Near Infra Red, Red, Green and Short-Wavelength Infra Red.

VI	**Formulation**	**Sensor**	**Type of variable**	**Reference**
NDVI	(NIR-R)/(NIR+R)	P,S,R	Vegetation productivity	(Tucker, 1979)
GDVI	NIR-G	P,S,R	Vegetation productivity	(Tucker, 1979)
MSAVI2	(2*NIR+1-sqrt((2*NIR+1)^2-8*(NIR-R)))/2	P,S,R	Vegetation productivity	(Qi et al., 1994)
PSRINIR	(R-B)/NIR	P,S,R	Vegetation productivity	(Merzlyak et al., 1999)
NDWI	(NIR-SWIR)/(NIR+SWIR)	S	Water stress	(Gao, 1996)
CIGreen	NIR/G-1	P,S,R	Nutrient stress	(Gitelson et al., 2003)

Table 2 Explanatory variables used in the gradient boosting tree (GBM) regression analysis. Parkland structure proxy used to estimate yield in the final model were discarded from the analysis to avoid redundancy of information.

Variable name	**Description**	**Unit**
Dependent		
Patch YH	Yield spatial variability	%
Independent		
Landscape Woody Cover	Mean woody cover in a 500 m buffer zone around the patch	%
Landscape Tree density	Mean tree density in in a 500 m buffer zone around the patch	Number/ha
Nutrient stress	Mean CIGreen over the growing season	Dimensionless
Water stress	Mean NDWI over the growing season	Dimensionless
Cover heterogeneity	Heterogeneity of crop cover over the growing season	Dimensionless
Soil texture	Category of soil texture	Type
Soil Organic Content	Total soil organic content in the 0-30 cm depth	‰
Total Nitrogen	Total soil organic nitrogen	ppm
Total Phosphorus	Total soil phosphorus	ppm